
Feature Attribution with Necessity and Sufficiency via Dual-stage Perturbation Test for Causal Explanation

Xuexin Chen¹ Ruichu Cai¹ Zhengting Huang¹ Yuxuan Zhu¹ Julien Horwood² Zhifeng Hao³ Zijian Li⁴
José Miguel Hernández-Lobato²

Abstract

We investigate the problem of explainability in machine learning. To address this problem, Feature Attribution Methods (FAMs) measure the contribution of each feature through a perturbation test, where the difference in prediction is compared under different perturbations. However, such perturbation tests may not accurately distinguish the contributions of different features, when their change in prediction is the same after perturbation. In order to enhance the ability of FAMs to distinguish different features' contributions in this challenging setting, we propose to utilize the Probability of Necessity and Sufficiency (PNS) that perturbing a feature is a necessary and sufficient cause for the prediction to change as a measure of feature importance. Our approach, Feature Attribution with Necessity and Sufficiency (FANS), computes the PNS via a perturbation test involving two stages (factual and interventional). In practice, to generate counterfactual samples, we use a resampling-based approach on the observed samples to approximate the required conditional distribution. We demonstrate that FANS outperforms existing attribution methods on six benchmarks. Our source code is available at <https://github.com/DMIRLAB-Group/FANS>.

1. Introduction

Feature attribution is a method for explaining machine learning (ML) models by assigning weights to input features,

^{*}Equal contribution ¹School of Computer Science, Guangdong University of Technology, Guangzhou 510006, China ²Department of Engineering, University of Cambridge, Cambridge CB2 1PZ, United Kingdom ³Shantou University, Shantou 515063, China ⁴Mohamed bin Zayed University of Artificial Intelligence, Masdar City, Abu Dhabi. Correspondence to: Ruichu Cai <cairuichu@gmail.com>.

where the absolute value of these weights denotes their contribution to a model's prediction. Mathematically, suppose we have a function f that denotes a trained ML model, a target input $\mathbf{x}^t = (x_1, \dots, x_d)$ to be explained, and a baseline $\mathbf{x}' = (x'_1, \dots, x'_d)$, where x'_i is the approximate value that feature x_i would take if it were considered missing. An attribution of the prediction at input \mathbf{x}^t relative to \mathbf{x}' is a vector $\alpha_f(\mathbf{x}^t, \mathbf{x}') = (a_1, \dots, a_d)$, where a_i is the contribution of x_i to the prediction $f(\mathbf{x}^t)$.

Standard feature attribution methods (FAMs) measure the contribution of each feature through a *perturbation* test, i.e., comparing the difference in prediction under different perturbations (e.g., Shapley Values (Shapley et al., 1953)), or before and after the perturbation (e.g., gradient or surrogate based methods (Lundberg & Lee, 2017; Sundararajan et al., 2017)), where a subset of the variables of \mathbf{X} are set to their baseline values.

However, this perturbation test may not accurately distinguish the contribution of different features to the prediction when their changes in prediction are similar after perturbation. To better understand this phenomenon, we provide an example as follows.

Example 1. Consider a binary classification model f for $\mathbf{X} = (X_1, X_2, X_3) \in \mathbb{R}^3$ that is captured by a function $Y = h(X_1, X_2, X_3) = \mathbb{I}(X_1 - X_2 > 1)$, where Y is a binary variable representing true or false. Assuming that the baseline \mathbf{x}' is $(0, 0, 0)$, given the target input $\mathbf{x}^t = (1, 1, 1)$.

The attribution scores obtained from the existing FAMs for features x_1 and x_3 may both be 0 since the model's predictions given \mathbf{x}^t under different perturbations relative to \mathbf{x}' are always equal to $h(\mathbf{x}^t)$, which may misleadingly suggest that x_1, x_3 contribute equally to $h(\mathbf{x}^t)$. Clearly, the contributions of x_1, x_3 are not equal, since the value of $h(\mathbf{x}^t)$ is determined solely by the difference between x_1 and x_2 being less than 1, and is not influenced by x_3 . In other words, the reasons why the predictions for x_1 and x_3 remain unchanged after being perturbed are different. Based on this key observation, we extend feature attribution to compare differences of each feature in a probability of causation, Probability of Necessity and Sufficiency (PNS,

as the “if and only if” of the relationship), by quantifying the probability of two counterfactual questions about x_3 (or x_2): “for all inputs with x_3 , and the predictions for these inputs remain unchanged when some features (except x_3) are perturbed, would the predictions change if x_3 were perturbed?” and “for all inputs with x_3 , and the predictions for these inputs change when only x_3 is perturbed, would the predictions remain unchanged if some features (except x_3) were perturbed?” The first question assesses the sufficiency of perturbing feature x_3 (cause A) for the prediction change (effect B), that is, the ability of cause A to produce effect B. Similarly, the second question assesses the necessity, that is, the dependence of effect B on cause A (Pearl, 2000). In Example 1, the PNS for x_3 is 0, since perturbing x_3 is impossible to cause the prediction to change, while the PNS for x_1 may be greater than 0 because the prediction may change when x_1 is perturbed.

Based on the understanding of the relationship between PNS and feature attribution mentioned above, we develop a novel subset-wise Feature Attribution with Necessity and Sufficiency (FANS) to quantify the PNS of the above two counterfactual questions about any feature subset of target input. Specifically, we abstract the common understanding of perturbation test in feature attribution by proposing a structural causal model (SCM). To quantify the counterfactual question, we then propose a novel dual-stage perturbation test to implement the counterfactual reasoning paradigm *Abduction-Action-Prediction* (Pearl, 2013). The first stage is to generate samples from a distribution condition on the factual perturbation and prediction of the counterfactual question (i.e., Abduction). The second stage involves perturbing the feature subset of each sample that differs from their factual perturbation (i.e., Action) and then updating the predictions. We implement two dual-stage perturbation tests specific to the counterfactual questions described above as the sufficiency module and necessity module of FANS, respectively. Finally, we separately calculated the proportion of the predictions of the necessity module that remained unchanged and the proportion of the prediction of the sufficiency module that changed. PNS can be estimated by calculating the weighted sum of these two proportions. However, the conditional distribution in the first stage may be complex, we thus propose to use Sampling-Importance-Resampling (DB, 1988) on the observed inputs to approximate it. Further, we combine FANS and a gradient-based optimization method to extract the subset with the largest PNS. We demonstrate FANS outperforms existing FAMs on six benchmarks of image and graph data.

2. Causal Model for Feature Attribution

In this section, we develop a principled framework to model the perturbation test in feature attribution, and describe the

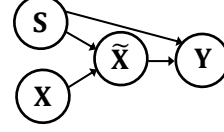


Figure 1. Causal diagram of standard perturbation test in feature attribution. S denotes a subset of dimensions of X for perturbation. \tilde{X} represents an input with fixed features on S that are similar to the target input x .

motivation of our proposed FANS approach that will be formally introduced in Section 3. The essential notations are presented in Appendix Table 4.

Structural Causal Model (SCM) for Standard Perturbation Test. In a SCM, all dependences are generated by functions that compute variables from other variables. In this paper, we take SCM as our starting point and try to develop everything from there. Figure 1 illustrates the causal diagram of standard perturbation test in feature attribution. Let X denote the d -dimensional input variable and S denote a subset of dimensions $\{1, 2, \dots, d\}$ of the input, with \bar{S} denoting its complement. Sequentially, define the conditional distribution of X with the condition that the L_p norm of the value of X on S with respect to the value of the target input x^t is not greater than a constant b . To avoid confusion, we represent the corresponding variable that follow this conditional distribution as \tilde{X} :

$$\tilde{X} \sim P(X \mid \|X_S - x_S^t\|_p \leq b). \quad (1)$$

In practice, we employ an empirical approximation of the distribution in Eq. 1 by sampling from the distribution of input given a value of S and retaining the samples that satisfy the condition $\|X_S - x_S^t\|_p \leq b$. We then observe the causal relationships $\tilde{X} \rightarrow Y$ and $S \rightarrow Y$. In this case, we perturb the features of \tilde{X} on S by a perturbation function g , and then feed the perturbed X into the model to generate a new prediction Y , which is denoted by

$$Y = f(g(\tilde{X}, S, x')). \quad (2)$$

Given a d -dimensional Bernoulli distribution with a user-specified hyperparameter φ (fixed to 0.5 in practice) and an all-ones vector $\mathbf{1}$, we implement the function g to randomly perturb the features of \tilde{X} specified by S as follows.

$$g(\tilde{X}, S, x') = (\mathbf{1} - \mathbf{m}_S) \circ \tilde{X}_S + \mathbf{m}_S \circ x'_S, \quad \mathbf{m} \sim \text{Bern}(\phi), \quad (3)$$

where \circ represents element-wise multiplication. The reason for the Bernoulli distribution introduced in Eq. 3 is that in the process of quantifying the model’s predictions by the impact of perturbing the dimensions specified by S , the dimensions that can influence the model predictions may be S or a subset of S . Therefore, we sample selected dimensions of S to obtain a more comprehensive quantification.

Goal of Standard Perturbation Test. A FAM using standard perturbation test aims to quantify the importance of a feature subset corresponding to \mathbf{s} (denoted by $a_{\mathbf{s}}$) which comprises two steps: (1) evaluate two model predictions of Y under different \mathbf{S} values (\mathbf{s} and \mathbf{s}') through the causal model mentioned above, where \mathbf{s}' used for reference is generally an empty set (i.e., no perturbation on \mathbf{X}); (2) compute the importance $a_{\mathbf{s}}$ by comparing the difference in predictions. Formally, $a_{\mathbf{s}}$ is given by a function $\phi : \mathcal{Y} \times \mathcal{Y} \rightarrow \mathcal{A}$ that maps two predictions in \mathcal{Y} to a scalar in $\mathcal{A} \subseteq \mathbb{R}$.

Remark 1. A variety of FAMs to implement perturbation test are compatible with our introduced causal model, contingent on their respective implementations of $\tilde{\mathbf{X}}$, g and ϕ . For example, the method of Shapley Values fixes the variable $\tilde{\mathbf{X}}$ to be target \mathbf{x}^t , define the score function ϕ to be Shapley Value, and let $\mathbf{s} := \mathbf{s} \cup x_i$ and $\mathbf{s}' := \mathbf{s}$.

Remark 2. Our causal model differs from the standard causal generation process in two ways. First, variable \mathbf{Y} is the model’s prediction rather than a property of the real-world data. Second, by intervening on a variable in our process, the outcome of its corresponding children’s variables is available.

3. Feature Attribution as a Problem of PNS Measurement

In Example 1, we demonstrate that the feature attribution method utilizing standard perturbation test mentioned in the previous section is limited in its ability to distinguish the importance of features when their degree of change in the prediction are similar.

To address this issue, our key finding is that the same change in prediction can be caused by different causes. Building upon this finding, we now formally introduce the method of calculating the probability related to the cause of each feature, namely PNS, which quantify the joint probability of two counterfactual questions about any feature subset. These counterfactual questions are both related to two key events that occurred in the process of $\tilde{\mathbf{X}}, \mathbf{S} \rightarrow Y$ in the perturbation test. Specifically, suppose we have an input \mathbf{x} , a subset of input dimensions \mathbf{s} and let \mathbf{y} denote the value of \mathbf{Y} after feeding them into the causal model (Eq.1-3). We denote $A_{\mathbf{s}}$ as an event of *perturbation on the subset \mathbf{s} of an input \mathbf{x} , which is represented by the perturbation $g(\mathbf{x}, \mathbf{s}, \mathbf{x}')$* (Eq. 3). We use $\bar{A}_{\mathbf{s}}$ to denote event $A_{\mathbf{s}}$ not occurring, which is represented by $\bar{A}_{\mathbf{s}} = \bigvee_{i=1}^{2^d-1} A_{\mathbf{s}'_i}$, where \mathbf{s}'_i represents a possible set of dimensions different from \mathbf{s} . Since 2^d-1 may be large, we use the complement of \mathbf{s} to approximate $\bar{A}_{\mathbf{s}}$, that is, $\bar{A}_{\mathbf{s}} \approx A_{\bar{\mathbf{s}}}$. We denote $B_{\mathbf{s}}$ as an event of *the change in the original prediction $f(\mathbf{x})$ relative to \mathbf{y} , which is represented by $|\mathbf{y} - f(\mathbf{x})| > c$* , where constant c is a hyperparameter. Similarly, $\bar{B}_{\mathbf{s}}$ is denoted as an event of $|\mathbf{y} - f(\mathbf{x})| \leq c$. Based

on these events, we provide the following definitions of counterfactual probabilities (Pearl, 2022).

Definition 3.1. (Probability of necessity, PN)

$$PN = P(\bar{B}_{\mathbf{s}\bar{A}_{\mathbf{s}}} | A_{\mathbf{s}}, B_{\mathbf{s}}), \quad (4)$$

PN represents the probability of the following counterfactual question: given that events $A_{\mathbf{s}}$ and $B_{\mathbf{s}}$ both occur initially, would event $B_{\mathbf{s}}$ do not occur if event $A_{\mathbf{s}}$ were changed from occurring to not occurring.

Definition 3.2. (Probability of sufficiency, PS)

$$PS = P(B_{\mathbf{s}A_{\mathbf{s}}} | \bar{A}_{\mathbf{s}}, \bar{B}_{\mathbf{s}}) \quad (5)$$

PS is the probability of the following counterfactual question: given that events $A_{\mathbf{s}}$ and $B_{\mathbf{s}}$ both did not occur initially, would event $B_{\mathbf{s}}$ occur if event A were changed from not occurring to occurring.

Definition 3.3. (Probability of necessity and sufficiency, PNS)

$$PNS = PN \cdot P(A_{\mathbf{s}}, B_{\mathbf{s}}) + PS \cdot P(\bar{A}_{\mathbf{s}}, \bar{B}_{\mathbf{s}}). \quad (6)$$

PNS is the weighted sum of PN and PS, each multiplied by the probability of its corresponding condition. PNS measures the probability that event $A_{\mathbf{s}}$ is a necessary and sufficient cause for event $B_{\mathbf{s}}$.

When evaluating the importance $w_{\mathbf{s}}$ of the input features on the dimension subset \mathbf{s} , if we hope that $w_{\mathbf{s}}$ can reflect the probability that perturbing \mathbf{x} on \mathbf{s} is a sufficient and necessary cause of the prediction $f(\mathbf{x})$ change, then this $w_{\mathbf{s}}$ is defined in Eq. 7, and an illustrative example is provided accordingly.

$$w_{\mathbf{s}} := PN \cdot P(A_{\mathbf{s}}, B_{\mathbf{s}}) + PS \cdot P(\bar{A}_{\mathbf{s}}, \bar{B}_{\mathbf{s}}). \quad (7)$$

Example 2. Consider a 1-dimensional model, $y = \sigma(x^2)$, with a target sample $x^t = 0.2$, a baseline $x' = 0$, $\mathbf{s} = \{1\}$, $b = 0.01$, and $c = 0.1$. Since $\bar{\mathbf{s}}$ is empty, the domain of definition of $P(\tilde{\mathbf{X}} | \bar{A}_{\mathbf{s}}, \bar{B}_{\mathbf{s}})$ is empty, thus we focus on calculating PN and $P(A_{\mathbf{s}}, B_{\mathbf{s}})$. And thus no perturbation will be performed when calculating PN. Consequently, PN is equal to 1. $P(A_{\mathbf{s}}, B_{\mathbf{s}})$ can be estimated through the empirical distribution of the dataset. Overall, the importance score of x^t is equal to $P(A_{\mathbf{s}}, B_{\mathbf{s}})$.

Therefore, in order to calculate the target score as shown in Eq. 7, it can be broken down into the calculation of four probabilities, where $P(A_{\mathbf{s}}, B_{\mathbf{s}})$ and $P(\bar{A}_{\mathbf{s}}, \bar{B}_{\mathbf{s}})$ are the observation probabilities, $P(\bar{B}_{\mathbf{s}} | A_{\mathbf{s}}, B_{\mathbf{s}})$ and $P(B_{\mathbf{s}} | \bar{A}_{\mathbf{s}}, \bar{B}_{\mathbf{s}})$ are the counterfactual probabilities PN and PS, respectively. According to the theory of counterfactual reasoning, PN and PS can be converted into the following equations for calculation (see the Appendix A for the detailed derivation).

$$\begin{aligned} & P(\bar{B}_{\mathbf{s}\bar{A}_{\mathbf{s}}} | A_{\mathbf{s}}, B_{\mathbf{s}}) \\ &= \mathbb{E}_{\mathbf{x} \sim P(\tilde{\mathbf{X}} | A_{\mathbf{s}}, B_{\mathbf{s}})} [P(|f(g(\mathbf{x}, \bar{\mathbf{s}}), \mathbf{x}')) - f(\mathbf{x})| \leq c)_{\text{do}(\tilde{\mathbf{X}}=\mathbf{x})}], \end{aligned} \quad (8)$$

$$P(B_{s_{A_s}} | \bar{A}_s, \bar{B}_s) = \mathbb{E}_{\mathbf{x} \sim P(\tilde{\mathbf{X}} | \bar{A}_s, \bar{B}_s)} [P(|f(g(\mathbf{x}, \mathbf{s}, \mathbf{x}')) - f(\mathbf{x})| > c)_{\text{do}(\tilde{\mathbf{X}}=\mathbf{x})}], \quad (9)$$

where $\text{do}(\tilde{\mathbf{X}}=\mathbf{x})$ denotes an intervention on variable $\tilde{\mathbf{X}}$ that fixes the value as \mathbf{x} (i.e., perform the *do*-calculus (Pearl, 2000)). In order to compute $P(\bar{B}_{s_{A_s}} | A_s, B_s)$ and $P(B_{s_{A_s}} | \bar{A}_s, \bar{B}_s)$, a novel dual-stage perturbation test will be proposed which implements the counterfactual reasoning paradigm (Pearl, 2013), as introduced in Section 4.

4. Necessary and Sufficient Attribution via Dual-stage Perturbation Test

4.1. Overview

Based on the definition of PNS, we propose a Feature Attribution with Necessity and Sufficiency (FANS) method to evaluate the PNS of each feature subset of the target input, as illustrated in Figure 2. In particular, we first develop a novel dual-stage (factual and interventional stage) perturbation test that allows us to estimate counterfactual probability. Subsequently, two dual-stage perturbation tests, one specific to PN and the other to PS, are implemented as the sufficiency and necessity modules of FANS, respectively. Finally, the outputs of these modules are combined to derive PNS. Since the conditional distributions involved in the factual stage may be complex, FANS employs the sampling-importance-resampling (SIR) method to approximate these distributions with observed samples. Furthermore, we also combine FANS with a gradient-based optimization method to extract the feature subset with the highest PNS.

4.2. Dual-stage Perturbation Test

We design two different dual-stage perturbation tests to estimate the PN in Eq. 8 and PS in Eq. 9, respectively, by following the Abduction-Action-Prediction counterfactual reasoning paradigm (Pearl, 2013). Abduction involves setting conditions for specific variables (corresponds to $\tilde{\mathbf{X}}$ in our context) based on the observations (corresponds to prediction \mathbf{Y} given the dimensions \mathbf{S}). The action involves intervening in the values of certain variables (corresponds to $\mathbf{S}, \tilde{\mathbf{X}}$). Prediction involves computing the resulting conditional predictive distribution. This corresponds to the conditional distribution for \mathbf{Y} given intervention value of \mathbf{S} and the factual values of $\tilde{\mathbf{X}}$.

We first present the dual-stage perturbation test for PS estimation. **1) (Factual stage)** Draw inputs from a distribution conditional on the fact that predictions remain unchanged after using the perturbation function (Eq. 3) to perturb the features of $\tilde{\mathbf{X}}$ on $\bar{\mathbf{s}}$ (i.e., events \bar{A}_s and \bar{B}_s both occur). **2) (Interventional stage)** Remove all arrows pointing to $\tilde{\mathbf{X}}$ in Figure 1. For each collected sample, use the perturbation function in Eq. 3 to randomly perturb on \mathbf{s} (i.e., event A_s

occur) and calculate the proportion of prediction changes (i.e., event B_s occur). Finally, average the proportion of prediction changes for each input. Similarly, the dual-stage perturbation test for PN estimation is constructed by exchanging the perturbations and prediction events involved in the above two stages respectively.

4.3. Sufficiency Module

This module provides a concrete implementation of the dual-stage perturbation test for PS estimation.

4.3.1. FACTUAL STAGE

To draw samples from $P(\tilde{\mathbf{X}} | \bar{A}_s, \bar{B}_s)$ in Eq. 9, we propose to apply SIR on the observed sample set \mathcal{E} that follows $P(\mathbf{X})$ to approximate the required conditional distribution. First, given perturbation $\bar{\mathbf{s}}$, the resampling weight for each observed sample is as follows (detailed derivation can be found in Appendix B). Letting r denote a normalization constant, the SIR-based resampling weight of $\mathbf{x} \sim P(\mathbf{X})$ is given by

$$w_{\text{SF}}(\mathbf{x}) = \begin{cases} r \cdot P(|f(g(\mathbf{x}, \bar{\mathbf{s}}, \mathbf{x}')) - f(\mathbf{x})| \leq c | \mathbf{x}), & \text{if } \|\mathbf{x}_{\bar{\mathbf{s}}} - \mathbf{x}_{\bar{\mathbf{s}}}^t\|_p \leq b \\ 0, & \text{otherwise.} \end{cases} \quad (10)$$

Hence, the resampling weight of \mathbf{x} is determined by two conditions: $\|\mathbf{x}_{\bar{\mathbf{s}}} - \mathbf{x}_{\bar{\mathbf{s}}}^t\|_p \leq b$ and $|f(g(\mathbf{x}, \bar{\mathbf{s}}, \mathbf{x}')) - f(\mathbf{x})| \leq c$. To enhance the smoothness of the output from $w_{\text{SF}}(\cdot)$, we introduce the Gaussian kernel function to soften the above two conditions and take their product as an approximation of $w_{\text{SF}}(\mathbf{x})$, as follows.

$$\tilde{w}_{\text{SF}}(\mathbf{x}) := \exp\left(\frac{\|\mathbf{x}_{\bar{\mathbf{s}}} - \mathbf{x}_{\bar{\mathbf{s}}}^t\|_p^2}{-2b^2}\right) \cdot \exp\left(\frac{|f(g(\mathbf{x}, \bar{\mathbf{s}}, \mathbf{x}')) - f(\mathbf{x})|^2}{-2c^2}\right), \quad (11)$$

where the thresholds b, c are used as the bandwidths of the Gaussian kernel. Further, we feed observed samples and their weight according to Eq. 11 into the SIR algorithm, and the sample set that approximates the conditional distribution $P(\tilde{\mathbf{X}} | \bar{A}_s, \bar{B}_s)$ in PS (Eq. 9) can be obtained.

4.3.2. INTERVENTION STAGE

Let \mathcal{E}_{SF} be a sample set draw from $P(\tilde{\mathbf{X}} | \bar{A}_s, \bar{B}_s)$, Then, PS (Eq. 9) can be estimated as follows:

$$\hat{\text{PS}} = \frac{1}{|\mathcal{E}_{\text{SF}}| \cdot t_{\text{SF}}} \sum_{\mathbf{x} \in \mathcal{E}_{\text{SF}}} \sum_{j=1}^{t_{\text{SF}}} \mathbb{I}(|f(g(\mathbf{x}, \mathbf{s}, \mathbf{x}')) - f(\mathbf{x})| > c), \quad (12)$$

where the constant t_{SF} is a hyperparameter and represents the number of times a random perturbation is applied to \mathbf{x} through the perturbation function g (Eq. 3).

4.4. Necessity Module

The implementation of the necessity module is similar to the sufficiency module, with the only difference being the

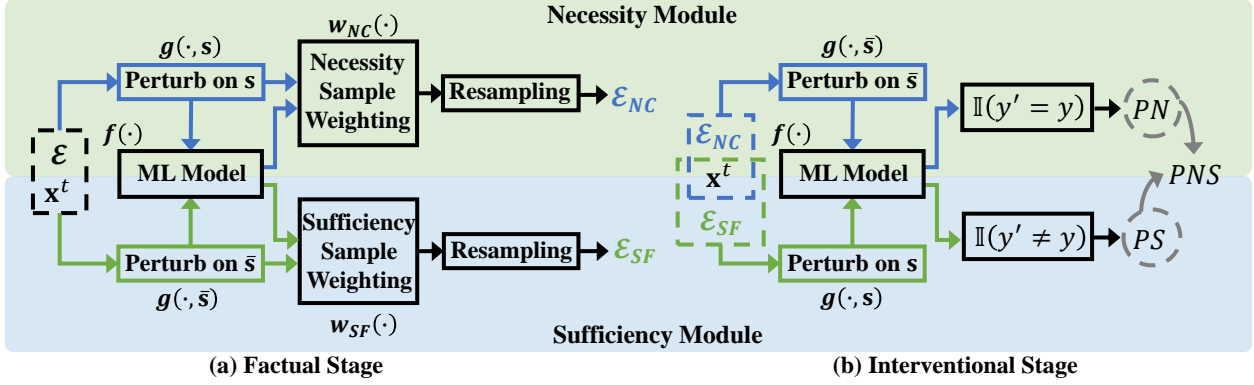


Figure 2. Architecture of FANS, which takes the sample \mathbf{x}^t to be explained and the samples $\mathcal{E} \stackrel{\text{iid}}{\sim} P(\mathbf{X})$ as inputs, throughout the necessity and sufficiency modules to output PN and PS, respectively, and finally combine PN, PS into PNS. Each module consists of the following two stages. 1) Factual stage. Generate samples \mathcal{E}_{NC} and \mathcal{E}_{SF} conditional on the fact that the model’s predictions change or remain unchanged respectively after performing perturbations on dimension subset \mathbf{s} and $\bar{\mathbf{s}}$. 2) Intervention stage. Apply perturbations different from the facts to \mathcal{E}_{SF} and \mathcal{E}_{NC} , and count the proportion of changes in the perturbed predictions \mathbf{y}' compared to the original prediction \mathbf{y} .

opposite given perturbation and prediction events in each stage. Thus, in the factual stage, the SIR-based resampling weight for the observed sample $\mathbf{x} \sim P(\mathbf{X})$, which is used to generate the sample set that approximates the conditional distribution $P(\tilde{\mathbf{X}}|A_{\mathbf{s}}, B_{\mathbf{s}})$ in Eq. 8, is given by

$$\tilde{w}_{\text{NC}}(\mathbf{x}) := \exp\left(\frac{\|\mathbf{x}_{\mathbf{s}} - \mathbf{x}_{\mathbf{s}}^t\|_p^2}{-2b^2}\right) \cdot \left(1 - \exp\left(\frac{|f(g(\mathbf{x}, \mathbf{s}, \mathbf{x}')) - f(\mathbf{x})|^2}{-2c^2}\right)\right). \quad (13)$$

Further, let \mathcal{E}_{NC} be a sample set of $P(\tilde{\mathbf{X}}|A_{\mathbf{s}}, B_{\mathbf{s}})$ obtained through SIR. Then PN (Eq. 8) can be estimated as follows:

$$\hat{\text{PN}} = \frac{1}{|\mathcal{E}_{\text{NC}}| \cdot t_{\text{NC}}} \sum_{\mathbf{x} \in \mathcal{E}_{\text{NC}}} \sum_{j=1}^{t_{\text{NC}}} \mathbb{I}(|f(g(\mathbf{x}, \bar{\mathbf{s}}, \mathbf{x}')) - f(\mathbf{x})| \leq c). \quad (14)$$

where the constant t_{NC} denotes the number of perturbations.

4.5. PNS Estimation

As indicated by Eq. 6, PNS are equivalent to the weighted sum of the PS and PN, with the weights being $P(A_{\mathbf{s}}, B_{\mathbf{s}})$ and $P(\bar{A}_{\mathbf{s}}, \bar{B}_{\mathbf{s}})$. The weights can be calculated as follows.

Consider the fact that $P(A_{\mathbf{s}}, B_{\mathbf{s}})$ (or $P(\bar{A}_{\mathbf{s}}, \bar{B}_{\mathbf{s}})$) can be expressed as the weighted sum of conditional probabilities $P(A_{\mathbf{s}}, B_{\mathbf{s}}|\mathbf{x})$ with respect to all possible \mathbf{x} , where the weight is $P(\mathbf{x})$. Hence, we can estimate $P(A_{\mathbf{s}}, B_{\mathbf{s}})$ and $P(\bar{A}_{\mathbf{s}}, \bar{B}_{\mathbf{s}})$ by summing their SIR-based weights of the observed samples in Eq. 13 and Eq. 11 respectively. In particular, given the sample set $\mathcal{E} \stackrel{\text{iid}}{\sim} P(\mathbf{X})$,

$$\hat{P}(A_{\mathbf{s}}, B_{\mathbf{s}}) = \sum_{\mathbf{x} \in \mathcal{E}} w_{\text{NC}}(\mathbf{x}), \quad \hat{P}(\bar{A}_{\mathbf{s}}, \bar{B}_{\mathbf{s}}) = \sum_{\mathbf{x} \in \mathcal{E}} w_{\text{SF}}(\mathbf{x}). \quad (15)$$

4.6. Extracting Feature Subset with the Highest PNS

In this section, we aim to efficiently extract the feature subset with the highest PNS in the target input. Specifically, we

use stochastic gradient descent to maximize the estimated PNS with respect to the dimension subset \mathbf{s} . Given the discrete nature of the dimension subset \mathbf{s} , we first encode it as a binary vector containing d dimensions, and then relax the entries in the discrete set $\{0, 1\}$ into the continuous range $[0, 1]$. Additionally, we use $\mathbf{1} - \mathbf{s}$ to represent the complement of \mathbf{s} , where $\mathbf{1}$ is an all-ones vector. Further, we replace $\|\mathbf{x}_{\mathbf{s}} - \mathbf{x}_{\mathbf{s}}^t\|_p$ in Eq. 11 with $\|\mathbf{x} \circ (\mathbf{1} - \mathbf{s}) - \mathbf{x}^t \circ (\mathbf{1} - \mathbf{s})\|_p$, where \mathbf{s} is now a relaxed binary vector and \circ is a element-wise multiplication. Similarly, we replace $(\mathbf{1} - \mathbf{m}_{\mathbf{s}}) \circ \tilde{\mathbf{X}}_{\mathbf{s}} + \mathbf{m}_{\mathbf{s}} \circ \mathbf{x}'_{\mathbf{s}}$ in Eq. 3 with $(\mathbf{1} - \mathbf{m}) \circ \tilde{\mathbf{X}} \circ \mathbf{s} + \mathbf{m} \circ \mathbf{x}' \circ \mathbf{s}$. In addition, the indicator function $\mathbb{I}(|f(\cdot) - f(\cdot)| > c)$ in Eq. 12 is not differentiable, thus we replace it with the smooth function $1 - \exp(-|f(\cdot) - f(\cdot)|)$ to indicate whether the prediction changes. Similarly, $\mathbb{I}(|f(\cdot) - f(\cdot)| \leq c)$ in Eq. 14 is replaced with $\exp(-|f(\cdot) - f(\cdot)|)$.

Finally, after the optimization with respect to \mathbf{s} is completed by maximizing Eq. 6, the resultant value of \mathbf{s} is utilized for the soft selection of the feature subset with the highest PNS.

4.7. Implementation of Thresholds b, c

The constants ‘ b ’ and ‘ c ’ in Eq. 11 and Eq. 13 represents the thresholds of similarity between inputs on some dimensions as well as between predictions, respectively. The robustness of the model is the main factor in determining the values of ‘ b ’ and ‘ c ’. However, since the model is a black box, FANS employs following heuristic methods to compute their values.

The value of ‘ b ’ is set to ensure that the neighborhood of \mathbf{x}^t is both small and nearly uniformly dense. Thus, the value of ‘ b ’ is then determined based on the Scott rule (Scott, 1979), a bandwidth estimation method widely used in kernel density estimation, which is given by $b = 1.06 \cdot |\mathcal{E}|^{\frac{1}{4+d}}$,

where $\mathcal{E} \stackrel{\text{iid}}{\sim} P(\mathbf{X})$ and d is the dimension of the input. On the other hand, the strategy for determining the c value is as follows. We first use the normal distribution $N(\mathbf{0}, \sigma^2 \cdot \mathbf{I})$ to simulate low-intensity noise, where σ is a small constant (we set it to 0.001 in practice), $\mathbf{0}$ is the all-zero vector, and \mathbf{I} is the identity matrix. Assuming that the model’s predictions for inputs with this noise are unchanged, we define the maximum variance of these predictions as $c := \max_{\mathbf{x} \in \mathcal{E}, \epsilon \in \mathcal{R}} |f(\mathbf{x}) - f(\mathbf{x} + \epsilon)|$, where $\mathcal{E} \stackrel{\text{iid}}{\sim} P(\mathbf{X})$, $\mathcal{R} \stackrel{\text{iid}}{\sim} N(\mathbf{0}, \sigma^2 \cdot \mathbf{I})$. Details regarding the sensitivity analysis of ‘b’ and ‘c’ are provided in Appendix E.

5. Experiments

5.1. Experimental Setup

1) **Datasets and models.** We utilized six public datasets with well-trained models: CIFAR10 (Krizhevsky et al., 2009) with ResNet18, MNIST (LeCun et al., 1998) and Fashion-MNIST (Xiao et al., 2017) with LeNet5, as well as BACommunity, Pubmed, and Citeseer with GCN (Ying et al., 2019; Sen et al., 2008; Kipf & Welling, 2016). CIFAR10, MNIST, and Fashion-MNIST are image datasets. BACommunity, Pubmed, and Citeseer are graph datasets. Please see Appendix C.1 for details.

2) **Baselines.** We selected the most popular or the most recent methods as the baseline. We then compared FANS with six feature-wise attribution methods: Saliency (Simonyan et al., 2013), GuidedBP (Springenberg et al., 2015), IntegratedGrad(IG) (Sundararajan et al., 2017), GradShap (Lundberg & Lee, 2017), DeepLift (Ancona et al., 2018), and IDGI (Yang et al., 2023), as well as twelve feature subset-wise attribution approaches: Occlusion (Zeiler & Fergus, 2014), LIME (Ribeiro et al., 2016), MeaningfulPerturb(MP) (Fong & Vedaldi, 2017), GNNExplainer (Ying et al., 2019), PGExplainer (Luo et al., 2020), FeatAblation (Kokhlikyan et al., 2020), ReFine (Wang et al., 2021), CFGNExplainer (Lucic et al., 2022), CF² (Tan et al., 2022), NSEG (Cai et al., 2022), CIMI (Wu et al., 2023) and MixUpExplainer (Zhang et al., 2023). The data categories used to test each baseline are largely aligned with their literature. Except that we adjust CIMI to accommodate image data, and run Saliency, GuidedBP, and IG on both graph and image data. Please see Appendix C.2 for details.

3) **Evaluation metrics.** We utilized six widely used metrics to evaluate the effectiveness of FANS: Infidelity(INF) (Yeh et al., 2019), Iterative Removal Of Features(IR) (Rieger & Hansen, 2020), Fidelity⁺(FID⁺), Fidelity⁻(FID⁻) (Amara et al., 2022), Max-Sensitivity(MS) (Yeh et al., 2019), Sparseness(SPA) (Chalasani et al., 2020), and Recall@12 (Wang et al., 2021) metrics. INF, IR, FID⁺, and FID⁻ measure the extent to which the explanation follows the predicted behavior of the model (i.e., faithfulness), while MS measures the

stability of the explanation when subjected to slight input perturbations (i.e., robustness) (Hedström et al., 2023). SPA measures the sparsity of the explanation by using the Gini Index. Recall@12 measures how many of the top 12 most important features for a given attribution are features of the “ground-truth explanation”. Remarkably, Recall@12 is only suitable for BACommunity since this dataset is synthetic and contains “ground-truth explanation”. Please see Appendix C.3 for details.

To test the explanation methods, we randomly selected 4,000 images from each image dataset (i.e., MNIST, Fashion-MNIST, and CIFAR10) and adopted the same configuration as the literature (Wang et al., 2021) on the graph datasets (i.e., BACommunity, Citeseer, and Pubmed). The results presented in Tables 1 and 2 are largely averages of the metric values for the different inputs, with the exception of FID⁺ and FID⁻, since these are metrics designed for the entire dataset rather than an individual sample. As each graph dataset we use contains only one graph, and FANS requires multiple samples for SIR, we create a graph-augmented dataset for each graph by randomly masking their adjacency matrix.

4) **Implementation details.** For the parametric explanation methods (MP, GNNExplainer, PGExplainer, ReFine, CFGNExplainer, CIMI, MixUpExplainer), we conducted a grid search to tune their hyperparameters.

Below are the details of our FANS. Since FANS belong to an feature subset-wise attribution method, we demonstrate the effectiveness of FANS by evaluating the feature subset with the highest PNS estimated by FANS through optimization w.r.t. dimension subset s (i.e., we adopt the setting of FANS introduced in Section 4.6). In practice, we utilized the Adam optimizer and set the learning rate to 0.001 for image datasets and 0.1 for graph datasets. The maximum number of training epochs was set to 50 for image datasets and 30 for graph datasets. The times of perturbation t_{SF} in Eq. 12 and t_{NC} in Eq. 14 were both set to 50. while the resampling sizes were set to 1. According to our proposed strategy in Section 4.7, the values of parameter b on MNIST, Fashion-MNIST, CIFAR10, BACommunity, Citeseer, and Pubmed are set to 1.0539, 1.0534, 1.0546, 1.0599, 1.0599 and 1.0600, respectively. Correspondingly, the parameter c are set to 0.0534, 0.0538, 0.0118, 7.0710×10^{-6} , 1.3271×10^{-6} and 4.0706×10^{-7} for the same datasets, respectively.

5.2. Explanation Evaluation

5.2.1. QUANTITATIVE EVALUATION

Performance comparison. We verify the experimental performance of FANS against the state-of-the-art baselines in Tables 1 and 2. As shown in Table 1, FANS significantly and consistently outperforms all the baselines in terms of faith-

Table 1. Performance on the image datasets. The best performance is marked in bold, and the second best is underlined. Symbols \uparrow and \downarrow respectively represent that larger and smaller metric values are better.

Method	MNIST				Fashion-MNIST				CIFAR10			
	INF \downarrow	IR \uparrow	SPA \uparrow	MS \downarrow	INF \downarrow	IR \uparrow	SPA \uparrow	MS \downarrow	INF \downarrow	IR \uparrow	SPA \uparrow	MS \downarrow
Saliency	3.8×10^4	64.3	0.658	0.623	1.8×10^6	25.5	0.558	0.753	1.2×10^8	54.1	0.492	0.736
IG	1.7×10^3	<u>73.3</u>	0.918	0.683	1.7×10^4	<u>60.8</u>	0.612	0.806	1.5×10^5	<u>63.5</u>	0.631	0.966
DeepLift	2.2×10^3	<u>73.3</u>	<u>0.918</u>	0.679	8.2×10^4	59.8	0.610	0.797	1.9×10^5	62.7	0.631	0.959
IDGI	2.0×10^3	64.7	0.837	0.578	2.6×10^4	58.2	0.593	0.781	2.3×10^4	19.5	<u>0.632</u>	0.854
GradShap	2.2×10^3	<u>73.3</u>	<u>0.918</u>	0.673	2.5×10^4	59.2	<u>0.614</u>	0.874	2.3×10^5	56.5	0.630	1.000
LIME	6.6×10^5	67.9	0.808	0.899	2.5×10^8	28.6	0.533	0.884	1.1×10^9	2.1	0.512	1.032
Occlusion	5.7×10^5	69.2	0.802	<u>0.538</u>	2.8×10^7	58.4	0.505	0.660	2.1×10^8	51.4	0.507	0.857
FeatAblation	1.7×10^3	72.8	0.917	0.669	5.5×10^4	45.4	0.572	0.791	1.1×10^6	36.8	0.619	0.983
MP	8.5×10^5	70.3	0.421	0.904	2.9×10^7	20.1	0.227	0.453	5.1×10^8	16.3	0.476	0.887
CIMI	1.7×10^4	12.9	0.901	0.548	2.6×10^4	54.8	0.589	0.827	6.0×10^6	21.1	0.589	<u>0.615</u>
FANS	9.0×10^2	74.5	0.924	0.463	1.2×10^4	63.1	0.630	<u>0.586</u>	1.7×10^4	63.6	0.634	0.578

fulness, sparsity, and robustness on different image datasets. In particular, we find that: 1) For the faithfulness metric INF, FANS outperforms the second-best approach by 47.06%, 29.41%, and 26.09% on MNIST, Fashion-MNIST, and CIFAR10. For IR, FANS improves by 1.64%, 3.78%, and 0.16%. These results indicate that extracting necessary and sufficient causes for input predictions can effectively capture key subsets of features that influence the model’s predictive behavior. 2) For the sparsity metric SPA, FANS outperforms the next best method by 0.65%, 2.61%, and 0.32% on the three image datasets. This validates that FANS’s necessity module, which adaptively removes unimportant features by randomly masking them, outperforms other methods in terms of attribution sparsity. 3) For the robustness metric MS, FANS outperforms the second-best method by 13.94% and 6.02% on the MNIST and CIFAR10 datasets, while achieving a somewhat lower but still competitive MS result on Fashion-MNIST. We find that FANS significantly outperforms gradient-based methods, probably due to the sensitivity of gradients to noisy feature values. FANS learns from a set of similar features obtained through SIR, which helps it to mitigate the effects of noise.

Similarly, in Table 2, FANS regularly surpasses all the baselines on the graph datasets. In particular, in terms of FID+, FANS improves by 4.99% on BACommunity, 46.15% on Citeseer, and 13.33% on Pubmed relative to the baselines. It provides further modest improvements with respect to the sparsity metric SPA. For another faithfulness metric FID-, FANS is the only method achieving optimal values (i.e., 0) across all three datasets. FANS outperforms other approaches for Citeseer and Pubmed while remaining competitive on Recall@12 for the synthetic BACommunity dataset.

Robustness analysis. Next, we investigate the robustness of FANS and the baseline methods by examining the effect of introducing noise. Following the literature (Yeh et al., 2019), we designed a robustness experiment as follows. Given various values of r , for $r \in [0, 1]$, we add noise to

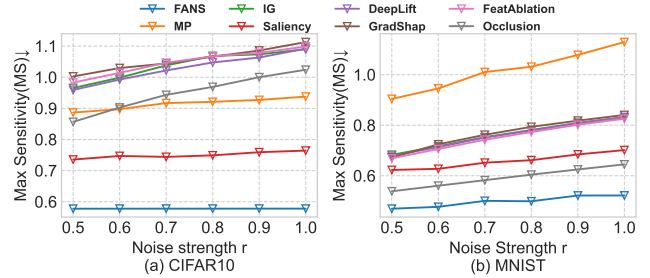


Figure 3. Performance on robustness comparison in image datasets CIFAR10 and MNIST under different strengths of noise r .

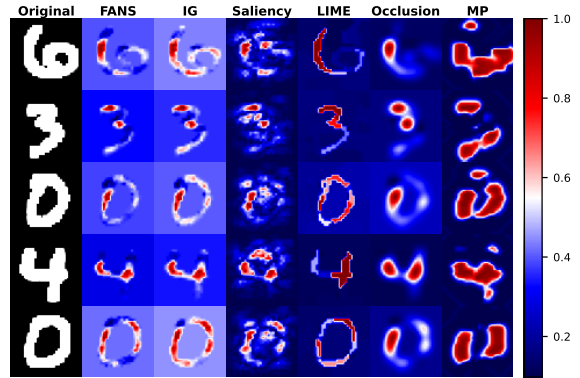


Figure 4. Attributions visualization on the MNIST dataset.

each pixel of input image \mathbf{x}_i from the interval $[-r, r]$. We then evaluate the difference between the explanations of each perturbed image and its original explanation via the Max Sensitivity (MS) metric. As shown in Fig.3(a)(b), as expected, all methods demonstrate a gradual deterioration in performance with increased noise strength. However, the slope of this deterioration is considerably lower using FANS, which demonstrates far superior robustness on both examined datasets. This can be explained by the fact that FANS learns from multiple samples which are similar to the target input through SIR, rather than a single sample, which renders it more robust to perturbation noise.

Table 2. Performance on the graph datasets.

Method	BACommunity				Citeseer			Pubmed		
	FID ⁺ ↑	FID ⁻ ↓	SPA↑	Recall@12↑	FID ⁺ ↑	FID ⁻ ↓	SPA↑	FID ⁺ ↑	FID ⁻ ↓	SPA↑
Saliency	0.6667	0.1000	0.8899	0.5141	0.1800	0.0400	0.7476	0.0250	0.0250	0.9670
GuidedBP	0.4833	0.1000	0.9137	0.3822	0.0607	0.1207	0.8410	0.0000	0.0250	0.9629
IG	0.6667	0.1167	0.9200	0.5204	0.5200	0.0400	0.8380	0.0250	0.0000	0.9636
GNNExplainer	0.4000	0.0667	0.6432	0.4210	0.1821	0.0000	0.3760	0.0750	0.0000	0.6058
PGExplainer	0.4667	0.0500	0.8092	0.6025	0.4292	0.2800	0.1435	0.0258	0.0250	0.01380
ReFine	0.4833	0.1500	0.4728	0.3208	0.2600	0.2600	0.4623	0.1055	0.1000	0.5890
CFGNEExplainer	0.5167	0.1500	0.7199	0.1987	0.5011	0.0000	0.5454	0.3751	0.0000	0.7048
CF ²	0.4667	0.0667	0.6216	0.6189	0.2200	0.0000	0.3706	0.1250	0.0000	0.5991
NSEG	0.5167	0.1000	0.6258	0.4806	0.1600	0.0000	0.3269	0.0750	0.0000	0.5757
MixUpExplainer	0.2333	0.1500	0.2064	0.3708	0.1200	0.0800	0.2963	0.0250	0.0750	0.1041
FANS	0.7000	0.0000	0.9311	0.5819	0.7600	0.0000	0.8619	0.4251	0.0000	0.9755

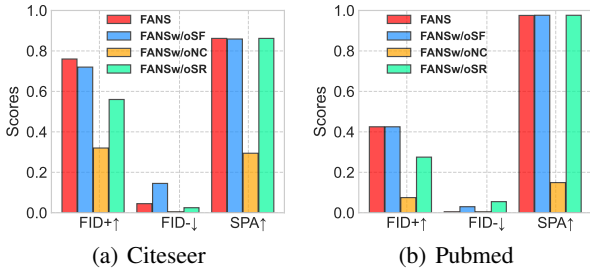


Figure 5. Ablation study of sufficiency (SF) module, necessity (NC) module, and SIR-based Sampling (SR) on graph datasets Citeseer and Pubmed.

5.2.2. QUALITATIVE EVALUATION

In Figure 4, we visualize the attributions obtained for FANS and other baselines on five samples from the MNIST dataset. We find that the attributions of FANS and IG are more sparse than other methods. Compared to IG, FANS improves the contrast between the scores of important and unimportant features. This is visually demonstrated by a higher number of blue pixels in FANS than in IG, which is expected since FANS’s PNS is used to attribute the sparsest and the most influential feature subset for the model’s predictions.

5.3. Ablation Study

The core components of FANS are the necessity, sufficiency, and SIR-based Sampling modules. In order to validate the importance of each component and better understand their relationship to different explainability metrics, we ablate our method by iteratively removing each component. We refer to FANS without the sufficiency module as FANSw/oSF, FANS without the necessity module as FANSw/oNC, and FANS without SIR-based Sampling as FANSw/oSR. We visualize the effects of this ablation on performance relative to the full algorithm in Figure 5 for the Citeseer and Pubmed datasets. In Figure 5(a)(b), we first remark that the full FANS algorithm is the only version of the method to perform uniformly well across both datasets and all met-

rics. When comparing with FANSw/oSF, we notice a slight decrease in the faithfulness metric FID+ and a significant decrease in FID-, while the sparsity metric remains stable, where FID- and FID+ evaluate the proportions of predictions remain unchanged and change when features with high attribution scores are retained and removed, respectively. Conversely, FANSw/oNC exhibits an opposite trend to the above three metrics of FANSw/oSF, with FID+ becoming significantly worse, FID- remaining stable, and SPA becoming worse. This result is expected since the sufficiency and necessity modules ensure that the feature subset contains all features responsible for the prediction and removes those that are not respectively, which result in a more dense or sparse optimal feature subset. Thus, the optimal subset estimated by FANSw/oSF may only contain a subset of features that are responsible for prediction. Removing these features may lead to prediction change (high FID+), while retaining these features may also lead to prediction change (high FID-) since the important features are incomplete. Similarly, the optimal subset estimated by FANSw/oNC may contain redundancy. Retaining these features may keep the prediction unchanged (low FID-) while removing these features the change in prediction is uncertain (low FID+) due to the redundancy.

Next, we compared FANS with FANSw/oSR. As shown in Figure 5(a)(b), the sparsity metric SPA of FANSw/oSR remains stable because of FANS’s necessity module. However, both faithfulness metrics FID+ and FID- decrease. This may be because FANSw/oSR lacks information of samples similar to the target input when learning the optimal subset of features, which may lead to FANS being affected by unimportant features of the target input.

5.4. Convergence Analysis

We corroborate the convergence analysis of FANS under different sizes of \mathcal{E} which are used for SIR-based resampling and show our FANS approaches a stationary point. Figure 6 shows the learning process of FANS with sample

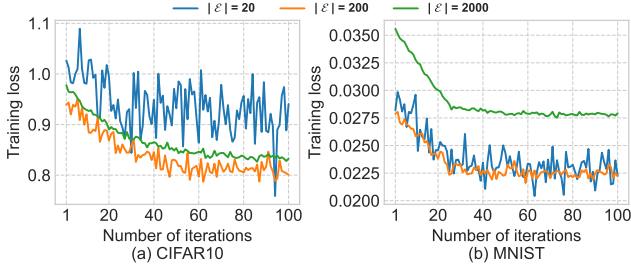


Figure 6. Convergence of FANS on datasets CIFAR10 and MNIST with sample sizes $|\mathcal{E}| = 20$, $|\mathcal{E}| = 200$ and $|\mathcal{E}| = 2,000$.

size $|\mathcal{E}| = 20$, $|\mathcal{E}| = 200$ and $|\mathcal{E}| = 2,000$. These values correspond to varying degrees of sparsity within the sample set \mathcal{E} . The training losses decreases with the number of iterations, leading to a convergent result in all cases. As shown in Figure 6 (a), we find that the training loss falls rapidly within the first 35 iterations, and begins to converge gradually in about 60 epochs. Figure 6 (b) shows that the model achieves earlier convergence within the first 30 iterations.

6. Related Work

Feature Attribution. Explainable artificial intelligence (XAI) methods aim to provide human-readable explanations to help users comprehend and trust the outputs created by ML models. At present, a series of XAI methods have been developed, mainly including building interpretable models (e.g., linear regression model) and generating post hoc explanations. Feature attribution methods (FAMs) (Nielsen et al., 2022; Yang et al., 2023), which provide an estimate of the contribution of input features to a model’s prediction, is one of the most popular post hoc techniques. In this paper, we restrict our attention to feature attribution. Existing FAMs mainly measure the contribution of features to prediction through a *perturbation* test, i.e., by perturbing the features and comparing the resulting differences in predictions. Typically, Shapley value-based methods (Shapley et al., 1953; Lundberg & Lee, 2017) measure the difference in a model’s predictions given data points with and without the feature included. Gradient-based methods (Sundararajan et al., 2017; Yang et al., 2023) measure the rate of change in prediction corresponding to a tiny change in an input feature. LIME-based methods (Ribeiro et al., 2016; Dhurandhar et al., 2022) learn simplified, interpretable models on perturbed feature subsets. In another line, subset-wise FAMs (e.g., GNNExplainer (Ying et al., 2019)) attempt to find a feature subset with the highest contribution by optimizing a loss function between the L_p norm of an feature mask and the prediction given the masked inputs (Fong & Vedaldi, 2017; Wang et al., 2021; Tan et al., 2022; Lucic et al., 2022; Zhang et al., 2023). However, current FAMs may not accurately distinguish the contributions between different features when their change in prediction is the

same after perturbation. To address this issue, we extend feature attribution to compare differences of each feature in PNS.

Probability of Necessity and Sufficiency (PNS). Necessity and sufficiency are two different aspects of causation. Sufficiency assesses the probability of a cause actively generating an effect, whereas necessity evaluates whether the cause, when absent, is capable of altering the effect, thereby measuring the effect’s dependence on the cause. At present, the main methods for feature attribution that consider sufficiency or necessity are LEWIS (Galhotra et al., 2021), LENS (Watson et al., 2021), and NSEG (Cai et al., 2022). However, since LEWIS and LENS only use PS or PN, the contribution score of an important feature subset may remain unchanged after including redundant features or removing some features inside. For example, we know that fuel, oxygen and heat cause burning. Since these three key factors and the ‘ice cream sold out’ (redundant feature) can also cause burning, $PS(\text{fuel, oxygen, heat}) = PS(\text{fuel, oxygen, heat, ‘ice cream sold out’})$. Another example is that without oxygen, burning doesn’t happen. Thus, $PN(\text{fuel, oxygen, heat}) = PN(\text{oxygen})$. NSEG extracts the feature subset with the largest PNS by introducing an identifiability assumption and then optimizing the lower bound of PNS, but our FANS does not require this assumption since we directly compute PNS according to its definition, hinging on our target outcome in the causal model is the model itself.

7. Conclusion

This paper presents a novel attribution method called Feature Attribution with Necessity and Sufficiency (FANS) that can better distinguish the contribution of different feature subsets to predictions. We first formally define the Structural Causality Model (SCM) for perturbation test, which is widely used by most existing feature attribution methods. Building upon this SCM, we propose to employ Probability of Necessity and Sufficiency (PNS) to measure the contribution of features to prediction via our proposed dual-stage perturbation test, which follows the Abduction-Action-Prediction counterfactual reasoning paradigm. To generate counterfactual samples, we propose to adopt a sampling-importance-resampling approach. Moreover, we show the superior performance of our FANS compared to state-of-the-art methods. The main limitation of our method is that FANS relies on multiple i.i.d. samples when explaining a target input, and thus FANS cannot be applied to models with only one training sample. In future work, an interesting direction would be to propose a new FANS method based on one-shot learning techniques.

Impact Statement

This paper proposes a feature attribution method called FANS, which can distinguish the contributions of different features even if the results change similarly after perturbation. FANS can be used in medical diagnosis, autonomous driving, and other fields to assist people in understanding the predictions of the model, which have the potential to facilitate the application of existing artificial intelligence technologies in real-world scenarios.

References

- Amara, K., Ying, Z., Zhang, Z., Han, Z., Zhao, Y., Shan, Y., Brandes, U., Schemm, S., and Zhang, C. Graphframex: Towards systematic evaluation of explainability methods for graph neural networks. In Rieck, B. and Pascanu, R. (eds.), *Learning on Graphs Conference, LoG 2022, 9-12 December 2022, Virtual Event*, volume 198 of *Proceedings of Machine Learning Research*, pp. 44. PMLR, 2022. URL <https://proceedings.mlr.press/v198/amara22a.html>.
- Ancona, M., Ceolini, E., Öztireli, C., and Gross, M. Towards better understanding of gradient-based attribution methods for deep neural networks. In *6th International Conference on Learning Representations, ICLR 2018, Vancouver, BC, Canada, April 30 - May 3, 2018, Conference Track Proceedings*. OpenReview.net, 2018. URL <https://openreview.net/forum?id=Sy21R9JAW>.
- Cai, R., Zhu, Y., Chen, X., Fang, Y., Wu, M., Qiao, J., and Hao, Z. On the probability of necessity and sufficiency of explaining graph neural networks: A lower bound optimization approach. *arXiv preprint arXiv:2212.07056*, 2022.
- Chalasanani, P., Chen, J., Chowdhury, A. R., Wu, X., and Jha, S. Concise explanations of neural networks using adversarial training. In *Proceedings of the 37th International Conference on Machine Learning, ICML 2020, 13-18 July 2020, Virtual Event*, volume 119 of *Proceedings of Machine Learning Research*, pp. 1383–1391. PMLR, 2020. URL <http://proceedings.mlr.press/v119/chalasanani20a.html>.
- DB, R. Using the sir algorithm to simulate posterior distributions. In *Bayesian statistics 3. Proceedings of the third Valencia international meeting, 1-5 June 1987*, pp. 395–402. Clarendon Press, 1988.
- Dhurandhar, A., Natesan Ramamurthy, K., and Shanmugam, K. Is this the right neighborhood? accurate and query efficient model agnostic explanations. *Advances in Neural Information Processing Systems*, 35:9499–9511, 2022.
- Fong, R. C. and Vedaldi, A. Interpretable explanations of black boxes by meaningful perturbation. In *Proceedings of the IEEE international conference on computer vision*, pp. 3429–3437, 2017.
- Galhotra, S., Pradhan, R., and Salimi, B. Explaining black-box algorithms using probabilistic contrastive counterfactuals. In *Proceedings of the 2021 International Conference on Management of Data*, pp. 577–590, 2021.
- He, K., Zhang, X., Ren, S., and Sun, J. Deep residual learning for image recognition. In *Proceedings of the IEEE conference on computer vision and pattern recognition*, pp. 770–778, 2016.
- Hedström, A., Weber, L., Krakowczyk, D., Bareeva, D., Motzkus, F., Samek, W., Lapuschkin, S., and Höhne, M. M. M. Quantus: An explainable ai toolkit for responsible evaluation of neural network explanations and beyond. *Journal of Machine Learning Research*, 24(34):1–11, 2023. URL <http://jmlr.org/papers/v24/22-0142.html>.
- Kipf, T. N. and Welling, M. Semi-supervised classification with graph convolutional networks. *arXiv preprint arXiv:1609.02907*, 2016.
- Kokhlikyan, N., Miglani, V., Martin, M., Wang, E., Al-sallakh, B., Reynolds, J., Melnikov, A., Kliushkina, N., Araya, C., Yan, S., et al. Captum: A unified and generic model interpretability library for pytorch. *arXiv preprint arXiv:2009.07896*, 2020.
- Krizhevsky, A., Hinton, G., et al. Learning multiple layers of features from tiny images. 2009.
- LeCun, Y., Bottou, L., Bengio, Y., and Haffner, P. Gradient-based learning applied to document recognition. *Proceedings of the IEEE*, 86(11):2278–2324, 1998.
- Lucic, A., Ter Hoeve, M. A., Tolomei, G., De Rijke, M., and Silvestri, F. Cf-gnnexplainer: Counterfactual explanations for graph neural networks. In *International Conference on Artificial Intelligence and Statistics*, pp. 4499–4511. PMLR, 2022.
- Lundberg, S. M. and Lee, S.-I. A unified approach to interpreting model predictions. *Advances in neural information processing systems*, 30, 2017.
- Luo, D., Cheng, W., Xu, D., Yu, W., Zong, B., Chen, H., and Zhang, X. Parameterized explainer for graph neural network. *Advances in neural information processing systems*, 33:19620–19631, 2020.
- Nielsen, I. E., Dera, D., Rasool, G., Ramachandran, R. P., and Bouaynaya, N. C. Robust explainability: A tutorial on gradient-based attribution methods for deep neural

- networks. *IEEE Signal Processing Magazine*, 39(4):73–84, 2022.
- Pearl, J. Causality: Models, reasoning, and inference, second edition. *Cambridge University Press*, 2000.
- Pearl, J. Structural counterfactuals: A brief introduction. *Cognitive science*, 37(6):977–985, 2013.
- Pearl, J. Probabilities of causation: three counterfactual interpretations and their identification. In *Probabilistic and Causal Inference: The Works of Judea Pearl*, pp. 317–372. 2022.
- Ribeiro, M. T., Singh, S., and Guestrin, C. ” why should i trust you?” explaining the predictions of any classifier. In *Proceedings of the 22nd ACM SIGKDD international conference on knowledge discovery and data mining*, pp. 1135–1144, 2016.
- Rieger, L. and Hansen, L. K. IROF: a low resource evaluation metric for explanation methods. *CoRR*, abs/2003.08747, 2020. URL <https://arxiv.org/abs/2003.08747>.
- Scott, D. W. On optimal and data-based histograms. *Biometrika*, 66(3):605–610, 1979.
- Sen, P., Namata, G., Bilgic, M., Getoor, L., Galligher, B., and Eliassi-Rad, T. Collective classification in network data. *AI magazine*, 29(3):93–93, 2008.
- Shapley, L. S. et al. A value for n-person games. 1953.
- Simonyan, K., Vedaldi, A., and Zisserman, A. Deep inside convolutional networks: Visualising image classification models and saliency maps. 2013.
- Springenberg, J. T., Dosovitskiy, A., Brox, T., and Riedmiller, M. A. Striving for simplicity: The all convolutional net. In Bengio, Y. and LeCun, Y. (eds.), *3rd International Conference on Learning Representations, ICLR 2015, San Diego, CA, USA, May 7-9, 2015, Workshop Track Proceedings*, 2015. URL <http://arxiv.org/abs/1412.6806>.
- Sundararajan, M., Taly, A., and Yan, Q. Axiomatic attribution for deep networks. In *International conference on machine learning*, pp. 3319–3328. PMLR, 2017.
- Tan, J., Geng, S., Fu, Z., Ge, Y., Xu, S., Li, Y., and Zhang, Y. Learning and evaluating graph neural network explanations based on counterfactual and factual reasoning. In *Proceedings of the ACM Web Conference 2022*, pp. 1018–1027, 2022.
- Wang, X., Wu, Y., Zhang, A., He, X., and Chua, T.-S. Towards multi-grained explainability for graph neural networks. *Advances in Neural Information Processing Systems*, 34:18446–18458, 2021.
- Watson, D. S., Gultchin, L., Taly, A., and Floridi, L. Local explanations via necessity and sufficiency: Unifying theory and practice. In *Uncertainty in Artificial Intelligence*, pp. 1382–1392. PMLR, 2021.
- Wu, C., Wang, X., Lian, D., Xie, X., and Chen, E. A causality inspired framework for model interpretation. In *Proceedings of the 29th ACM SIGKDD Conference on Knowledge Discovery and Data Mining*, pp. 2731–2741, 2023.
- Xiao, H., Rasul, K., and Vollgraf, R. Fashion-mnist: a novel image dataset for benchmarking machine learning algorithms. *arXiv preprint arXiv:1708.07747*, 2017.
- Yang, R., Wang, B., and Bilgic, M. Idgi: A framework to eliminate explanation noise from integrated gradients. In *Proceedings of the IEEE/CVF Conference on Computer Vision and Pattern Recognition*, pp. 23725–23734, 2023.
- Yeh, C.-K., Hsieh, C.-Y., Suggala, A., Inouye, D. I., and Ravikumar, P. K. On the (in) fidelity and sensitivity of explanations. *Advances in Neural Information Processing Systems*, 32, 2019.
- Ying, Z., Bourgeois, D., You, J., Zitnik, M., and Leskovec, J. Gnnexplainer: Generating explanations for graph neural networks. *Advances in neural information processing systems*, 32, 2019.
- Zeiler, M. D. and Fergus, R. Visualizing and understanding convolutional networks. In *Computer Vision—ECCV 2014: 13th European Conference, Zurich, Switzerland, September 6-12, 2014, Proceedings, Part I 13*, pp. 818–833. Springer, 2014.
- Zhang, J., Luo, D., and Wei, H. Mixupexplainer: Generalizing explanations for graph neural networks with data augmentation. In *Proceedings of the 29th ACM SIGKDD Conference on Knowledge Discovery and Data Mining*, pp. 3286–3296, 2023.

Table 3. Statistics of the datasets.

Category	Dataset	# Images	Size	# Classes	
Image	MNIST	70,000	28×28	10	
	Fashion-MNIST	70,000	28×28	10	
	CIFAR10	60,000	32×32	10	
		# Nodes	# Edges	# Features	
Graph	BACommunity	1,400	8,598	10	8
	Citeseer	3,327	4,732	3,703	6
	Pubmed	19,717	44,338	500	3

A. Evaluation of PN and PS

As illustrated in Figure 1, the causal diagram demonstrates that variable \mathbf{Y} is influenced by variables $\tilde{\mathbf{X}}$ and \mathbf{S} , with a function of $\mathbf{Y} = f(g(\tilde{\mathbf{X}}, \mathbf{S}, \mathbf{x}'))$ (Eq. 2). When variables $\tilde{\mathbf{X}}$ and \mathbf{S} are intervened as \mathbf{x} and $\bar{\mathbf{s}}$ respectively, according to the counterfactual reasoning paradigm (Pearl, 2022), we have:

$$P(\bar{B}_{\mathbf{s}_{\bar{A}_{\mathbf{s}}}} \mid A_{\mathbf{s}}, B_{\mathbf{s}}) = \mathbb{E}_{\mathbf{x} \sim P(\tilde{\mathbf{X}} \mid A_{\mathbf{s}}, B_{\mathbf{s}})} \left[P(|\mathbf{Y} - f(\mathbf{x})| \leq c)_{\text{do}(\tilde{\mathbf{X}}=\mathbf{x}, \mathbf{S}=\bar{\mathbf{s}})} \right]$$

For simplicity, we replace \mathbf{Y} with its value $f(g(\tilde{\mathbf{X}} = \mathbf{x}, \mathbf{S} = \bar{\mathbf{s}}, \mathbf{x}'))$, and since \mathbf{S} is an exogenous variable, the above equation can be written as

$$= \mathbb{E}_{\mathbf{x} \sim P(\tilde{\mathbf{X}} \mid A_{\mathbf{s}}, B_{\mathbf{s}})} \left[P(|f(g(\mathbf{x}, \bar{\mathbf{s}}, \mathbf{x}')) - f(\mathbf{x})| \leq c)_{\text{do}(\tilde{\mathbf{X}}=\mathbf{x})} \right]$$

Similarly, the concise derivation of Eq. 9 is given by

$$\begin{aligned} P(B_{\mathbf{s}_{A_{\mathbf{s}}}} \mid \bar{A}_{\mathbf{s}}, \bar{B}_{\mathbf{s}}) &= \mathbb{E}_{\mathbf{x} \sim P(\tilde{\mathbf{X}} \mid \bar{A}_{\mathbf{s}}, \bar{B}_{\mathbf{s}})} [P(|\mathbf{Y} - f(\mathbf{x})| > c)_{\text{do}(\tilde{\mathbf{X}}=\mathbf{x}, \mathbf{S}=\mathbf{s})}] \\ &= \mathbb{E}_{\mathbf{x} \sim P(\tilde{\mathbf{X}} \mid \bar{A}_{\mathbf{s}}, \bar{B}_{\mathbf{s}})} [P(|f(g(\mathbf{x}, \mathbf{s}, \mathbf{x}')) - f(\mathbf{x})| > c)_{\text{do}(\tilde{\mathbf{X}}=\mathbf{x})}] \end{aligned}$$

B. Resampling Weight for Approximate Sampling

SIR consists of three steps. 1) Draw samples $\mathbf{x}_1, \dots, \mathbf{x}_k$ from the proposal distribution $Q(\mathbf{X})$. 2) For each \mathbf{x}_i , calculate the weight $w(\mathbf{x}_i) = \frac{P(\mathbf{x}_i \mid \bar{A}_{\mathbf{s}}, \bar{B}_{\mathbf{s}})}{Q(\mathbf{x}_i)}$ if $\|\mathbf{x}_{\bar{\mathbf{s}}} - \mathbf{x}_{\bar{\mathbf{s}}}^t\|_p \leq b$ (definition of variable $\tilde{\mathbf{X}}$ in Eq. 1) and 0 otherwise. 3) Draw samples from $\mathbf{x}_1, \dots, \mathbf{x}_k$ based on the their weights.

Next, we propose a method for estimating $\frac{P(\mathbf{x}_i \mid \bar{A}_{\mathbf{s}}, \bar{B}_{\mathbf{s}})}{Q(\mathbf{x}_i)}$. As the training set of the ML model comes from $P(\mathbf{X})$, we set $Q(\mathbf{X}) := P(\mathbf{X})$, thus $w(\mathbf{x}_i) = \frac{P(\mathbf{x}_i \mid \bar{A}_{\mathbf{s}}, \bar{B}_{\mathbf{s}})}{P(\mathbf{x}_i)} = \frac{P(\mathbf{x}_i)P(\bar{A}_{\mathbf{s}}, \bar{B}_{\mathbf{s}} \mid \mathbf{x}_i)}{P(\mathbf{x}_i)P(\bar{A}_{\mathbf{s}}, \bar{B}_{\mathbf{s}})} = \frac{P(\bar{A}_{\mathbf{s}}, \bar{B}_{\mathbf{s}} \mid \mathbf{x}_i)}{P(\bar{A}_{\mathbf{s}}, \bar{B}_{\mathbf{s}})} = r \cdot P(\bar{A}_{\mathbf{s}}, \bar{B}_{\mathbf{s}} \mid \mathbf{x}_i)$, where r is a normalization constant. Because $\bar{A}_{\mathbf{s}}$ denote an event of perturbation on any dimension subset (except \mathbf{s}) of an input \mathbf{x} . In our paper, we approximate this event by the complementary feature set $\bar{\mathbf{s}}$, which is represented by the perturbation $g(\mathbf{x}, \bar{\mathbf{s}}, \mathbf{x}')$. $\bar{B}_{\mathbf{s}}$ denote an event of the original prediction $f(\mathbf{x})$ remained unchanged relative to \mathbf{y} , which is represented by $|\mathbf{y} - f(\mathbf{x})| \leq c$, where constant c is a hyperparameter. Thus, $P(\bar{A}_{\mathbf{s}}, \bar{B}_{\mathbf{s}} \mid \mathbf{x}_i) = P(|f(g(\mathbf{x}_i, \bar{\mathbf{s}}, \mathbf{x}')) - f(\mathbf{x}_i)| \leq c \mid \mathbf{x}_i)$.

C. Experimental Setup

C.1. Datasets and Target Models

To evaluate the effectiveness of our proposed FANS, we utilize six datasets with well-trained black box models to be explained on image and graph domains: (1) on three image datasets (MNIST, Fashion-MNIST, CIFAR10), we train three image classification models using LeNet5 architecture (LeCun et al., 1998) for the first two datasets and ResNet18 (He et al., 2016) for the third dataset, and (2) on two citation graphs (Citeseer, Pubmed) and one synthetic graph (BACommunity), we train three node classification models, each consisting of three GCN (Kipf & Welling, 2016) layers, following (Wang et al., 2021). Table 3 summarizes the statistics of six datasets.

- **MNIST** (LeCun et al., 1998) contains grayscale images of the 10 digits.

- **Fashion-MNIST** (Xiao et al., 2017) contains grayscale images of the 10 categories.
- **CIFAR10** (Krizhevsky et al., 2009) contains colour images of the 10 categories.
- **BACommunity** (Ying et al., 2019) consists of two BA-Shapes graphs and includes eight node categories. A BA-Shapes graph contains a Barabási-Albert (BA) graph and “house”-structured network motifs.
- **Citeseer** and **Pubmed** (Sen et al., 2008) contain documents represented by nodes and citation links represented by edges.

C.2. Baselines

We consider two categories of methods, feature-wise attributions and feature subset-wise attributions. Feature-wise attribution methods include:

- **Saliency**(Simonyan et al., 2013) construct contributions using absolute values of partial derivatives.
- **GuidedBP**(Springenberg et al., 2015) sets the gradients and ReLU inputs to zero if they are negative.
- **IntegratGrad**(Sundararajan et al., 2017) average gradients along a linear path between the reference and input.
- **GradShap**(Lundberg & Lee, 2017) approximates SHAP values by stochastic sampling from the reference distribution and computing the expectations of gradients.
- **DeepLift**(Ancona et al., 2018) addresses saturation issues by employing “reference activations” computed during the forward pass with the reference input.
- **IDGI**(Yang et al., 2023) enhances attribution quality by removing noise in IG-based methods through focused use of gradients along the important direction.

Feature subset-wise attribution methods include:

- **Occlusion** (Zeiler & Fergus, 2014) induces changes in the classifier output through perturbation via sliding a gray square over the input image.
- **LIME** (Ribeiro et al., 2016) quantifies the contributions by using a simplified, interpretable surrogate by fitting the input’s neighborhood.
- **MeaningfulPerturbation(MP)**(Fong & Vedaldi, 2017) optimizes the shape of perturbation masks to minimize input image blurring while maximizing class score decrease.
- **GNNExplainer** (Ying et al., 2019) minimizes the loss by balancing the density penalty and cross-entropy of model prediction on the masked subgraph.
- **PGExplainer** (Luo et al., 2020) extends GNNExplainer by assuming a random Gilbert graph, where edge probabilities are conditionally independent.
- **FeatAblation** (Kokhlikyan et al., 2020) computes attribution by replacing each input feature with a reference and measuring the output difference.
- **ReFine** (Wang et al., 2021) involves edge attribution through pre-training, which optimizes mutual information (MI) and contrastive loss, and edge selection through fine-tuning, which solely maximizes MI.
- **CFGNEExplainer** (Lucic et al., 2022) generates counterfactual explanations by learning a perturbed adjacency matrix that flips the classifier prediction for a node.
- **CF²** (Tan et al., 2022) proposes an objective function for optimizing the edge mask, which consists of factual loss, counterfactual loss, and L_1 regularization.

- **NSEG** (Cai et al., 2022) uses SCMs for counterfactual probability estimation and optimizes continuous masks via gradient updates, using the PNS lower bound as the objective to generate necessary and sufficient GNN explanations.
- **CIMI** (Wu et al., 2023) minimizes the loss by balancing their proposed sufficiency loss, intervention loss, and causal prior loss.
- **MixUpExplainer** (Zhang et al., 2023) mixes explanations with a randomly sampled base structure to address distribution shifting issues.

C.3. Evaluation Metrics

It is challenging to evaluate the quality of explanations quantitatively because the ground truth explanations are usually not available. There are six widely used metrics in the literature.

C.3.1. INFIDELITY (INF)

The Infidelity (INF) metric (Yeh et al., 2019) quantifies the expected mean square error between the dot product of an attribution vector and the difference of input and perturbed input, and the difference of output before and after perturbations. Mathematically, Infidelity is defined as follows.

$$\text{INF}(\mathbf{s}, \mathbf{x}, f) = \mathbb{E}_{\mathbf{m} \sim U(\mathbf{0}, \mathbf{1})} \left[\left((\mathbf{x} - \mathbf{x} \circ \mathbf{m})^T \mathbf{s} - (f(\mathbf{x}) - f(\mathbf{x} \circ \mathbf{m})) \right)^2 \right],$$

where $\mathbf{x} \in \mathbb{R}^D$ is a target input to be explained, $U(\mathbf{0}, \mathbf{1})$ denotes the uniform distribution over the hypercube $[0, 1]^D$ in D -dimensional space, $\mathbf{s} \in \mathbb{R}^D$ represent the attribution vector determined by a FA method.

C.3.2. IROF (IR)

Iterative Removal Of Features (IROF or IR) (Rieger & Hansen, 2020) calculates the Area Over the Curve (AOC) for the class score based on the sorted mean importance of feature segments as they are iteratively removed. Formally, IROF is defined as follows.

$$\text{IROF}(\mathbf{a}_1, \dots, \mathbf{a}_N, \mathbf{x}_1, \dots, \mathbf{x}_N, f) = \frac{1}{N} \sum_{n=1}^N \text{AOC} \left(\frac{f(t(\mathbf{x}_n, \mathbf{a}_n, 1))_i}{f(\mathbf{x})_i}, \dots, \frac{f(t(\mathbf{x}_n, \mathbf{a}_n, L))_i}{f(\mathbf{x})_i} \right),$$

where i is a class index, L is the number of segments, \mathbf{x}_n represents the n -th target input to be explained, \mathbf{a}_n denotes the attribution of \mathbf{x}_n predicted by the feature attribution method to be evaluated. $t(\mathbf{x}_n, \mathbf{a}_n, l)$ is designed to perturb the input \mathbf{x}_n in a segment-wise manner. IROF calculates the importance of each segment in \mathbf{x}_n by averaging the significance scores of individual features within those segments, as provided by its attribution \mathbf{a}_n . The segments are then sorted based on their importance scores in descending order. Function t selectively perturbs the l -th ranked segment, yielding the modified input as its output.

C.3.3. FIDELITY⁺ (FID+) AND FIDELITY⁻ (FID-)

Fidelity⁺ metric (FID+) and Fidelity⁻ metric (FID-) (Amara et al., 2022) respectively evaluate the proportions of predictions changing and remaining unchanged when features with high attribution scores are removed and retained. For the sake of convenience in discussion, we assume that f is a multi-class classification model.

$$\text{Fidelity}^+(\mathbf{s}_1, \dots, \mathbf{s}_N, \mathbf{x}_1, \dots, \mathbf{x}_N, f) = 1 - \frac{1}{N} \sum_{i=1}^N \mathbb{I} \left(\arg \max_i f(\mathbf{x}) = \arg \max_i f(\mathbf{x} \circ (\mathbf{1} - \mathbf{s})) \right), \quad (16)$$

$$\text{Fidelity}^-(\mathbf{s}_1, \dots, \mathbf{s}_N, \mathbf{x}_1, \dots, \mathbf{x}_N, f) = 1 - \frac{1}{N} \sum_{i=1}^N \mathbb{I} \left(\arg \max_i f(\mathbf{x}) = \arg \max_i f(\mathbf{x} \circ \mathbf{s}) \right), \quad (17)$$

where $\arg \max_i f(\mathbf{x})$ denotes the category with the maximum predicted probability for a given input vector \mathbf{x} , where $f(\mathbf{x})$ represents the model's output, typically a vector of class probabilities.

C.3.4. MAX-SENSITIVITY (MS)

Max-Sensitivity (MS) (Yeh et al., 2019) computes the maximum difference between new and original attributions, where the new attributions correspond to perturbed inputs. Given a input neighborhood radius r and an attribution method h , the max-sensitivity is defined as:

$$\text{SENS}_{\text{MAX}}(h, \mathbf{x}, f, r) = \max_{\|\mathbf{z} - \mathbf{x}\| \leq r} \|h(f, \mathbf{z}) - h(f, \mathbf{x})\|. \quad (18)$$

C.3.5. SPARSENESS (SPA)

The Sparseness (SPA) metric (Chalasanani et al., 2020) is utilized to quantify the sparsity of an attribution, leveraging the Gini index on the absolute values of the attribution scores. Specifically, given a feature attribution \mathbf{s}^{sort} sorted in descending order, the Gini Index is given by

$$\text{Gini}(\mathbf{s}^{\text{sort}}) = 1 - 2 \sum_{d=1}^D \frac{s_d}{\|\mathbf{s}\|_1} \left(\frac{D - d + 0.5}{D} \right) \quad (19)$$

C.3.6. RECALL@N

Recall@N (Wang et al., 2021) is computed as $\mathbb{E}_G [|\mathcal{G}_s \cap \mathcal{G}_s^*| / |\mathcal{G}_s^*|]$, where \mathcal{G}_s^* is the ground-truth explanatory subgraph. Note that Recall@N in this paper is only suitable for BACommunity since it is a synthetic dataset with known motifs.

C.4. Implementation Details

For the parametric explanation methods (MP, GNNExplainer, PGExplainer, ReFine, CFGNExplainer, CIMI, MixUpExplainer), we conducted a grid search to tune their hyperparameters.

Below are the details of our FANS. Since FANS belong to an feature subset-wise attribution method, we demonstrate the effectiveness of FANS by evaluating the feature subset with the highest PNS estimated by FANS through optimization w.r.t. dimension subset \mathbf{s} (i.e., we adopt the setting of FANS introduced in Section 4.6). In practice, we utilized the Adam optimizer and set the learning rate to 0.001 for image datasets and 0.1 for graph datasets. The maximum number of training epochs was set to 50 for image datasets and 30 for graph datasets. The times of perturbation t_{SF} in Eq. 12 and t_{NC} in Eq. 14 were both set to 50. while the resampling sizes were set to 1. According to our proposed strategy in Section 4.7, the values of parameter b on MNIST, Fashion-MNIST, CIFAR10, BACommunity, Citeseer, and Pubmed are set to 1.0539, 1.0534, 1.0546, 1.0599, 1.0600, respectively. Correspondingly, the parameter c are set to 0.0534, 0.0538, 0.0118, 7.0710×10^{-6} , 1.3271×10^{-6} and 4.0706×10^{-7} for the same datasets, respectively.

D. Efficiency Analysis

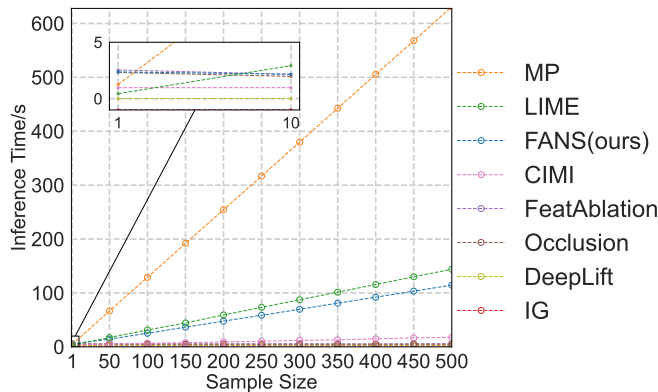


Figure 7. Efficiency analysis on the CIFAR10 dataset.

We evaluate the efficiency of FANS on CIFAR10, in terms of the inference time. We select representative baselines, including optimization-based methods MP, LIME, and CIMI, as well as non-optimization-based methods FeatAblation, Occlusion, DeepLift, and IG.

Table 4. Notation and Descriptions.

Notations	Descriptions
f and g	The black box model and perturbation function.
\mathbf{X} and \mathbf{Y}	The input and output variables of the model.
\mathbf{x}	A particular value of \mathbf{X} .
\mathbf{x}'	A baseline for perturbation.
\mathbf{x}^t ,	Target input to be explained
$\tilde{\mathbf{X}}$	Input with fixed features on \mathbf{S} that are similar to \mathbf{x} .
y	Prediction output by f given the input \mathbf{x} , i.e., $f(\mathbf{x})$.
y'	Prediction of f given the perturbed input.
\mathbf{m}	A random mask used to perturb the input.
\mathbf{S}	A set containing the dimensions of \mathbf{X} specified to be perturbed. \mathbf{S} can be any set and is not fixed.
\mathbf{s}	A particular example of \mathbf{S} , indicating the dimensions of the actual perturbation.
$\mathbf{x}_s, \mathbf{m}_s$	Subvectors of \mathbf{x} and \mathbf{m} that are indexed by \mathbf{s} .
A_s, \bar{A}_s	Perturbation event and its complement.
B_s, \bar{B}_s	Prediction event and its complement.
b	Threshold used to determine the similarity of the input to the target input in a specific dimension.
c	Threshold used to determine the similarity of the prediction after perturbation to the original prediction.
r, d	Normalization constant and the dimensionality of the input.
t, u	Number of perturbations in the sufficiency and necessity modules, respectively.
w_{SF} and w_{NC}	Sample weighting functions for PS and PN, respectively.
\mathcal{E}_{SF} and \mathcal{E}_{NC}	Sample sets drawn from conditional distributions of PS and PN through SIR, respectively.
$\mathbb{I}(\cdot)$ and \circ	Indicator function and element-wise multiplication.

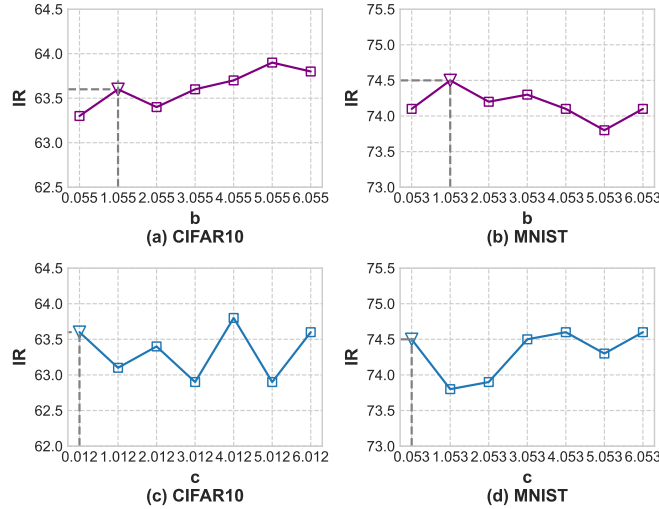


Figure 8. Parameter sensitivity analysis for FANS in Eq. 11 and Eq. 13.: (a)-(b) feature similarity threshold b . (c)-(d) prediction similarity threshold c . The triangle ‘ ∇ ’ represent the values of b or c that we obtained using our heuristic strategy.

As shown in Figure 7, the following two main conclusions can be drawn. First, for the same sample size, FANS remains competitive in terms of inference time. Second, for the same time, when the time is approximately greater than 10 seconds, FANS can explain more samples than MP and LIME in the same amount of time. For instance, when given an inference time of 100 seconds, FANS can process approximately 450 samples, whereas LIME and MP can only handle around 350 and 75 samples, respectively. Note that the efficiency of FeatAblation, Occlusion, DeepLift, and IG remains stable, which is expected since they simply compute gradients or perturbations for each sample.

E. Sensitivity Analysis of Thresholds b and c

We present the sensitivity analysis for the parameters b and c in our FANS. Figure 8 (a) and (b) show that the performance of FANS is not sensitive to changes in the values of b . In particular, values of $b = 1.055$ on CIFAR10 and $b = 1.053$ on MNIST computed by our proposed heuristic strategy in Section 4.7 typically give robust and comparable performance. For the value of c , the performance of FANS gradually decreases and becomes stable, with the value of $c = 0.012$ on CIFAR10 and $c = 0.053$ on MNIST also giving comparable performance.